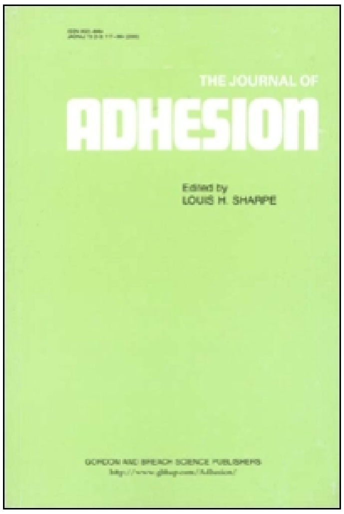

The Journal of Adhesion
Publication details, including instructions for authors and subscription information:
http://www.informaworld.com/smpp/title~content=t713453635

Nickel Activated Phosphating of Cold-Rolled Steel

H. W. K. Ong[a]; L. M. Gan[a]; T. L. Tan[a]
[a] Chemistry Department, National University of Singapore, Republic of Singapore

To cite this Article Ong, H. W. K. , Gan, L. M. and Tan, T. L.(1986) 'Nickel Activated Phosphating of Cold-Rolled Steel', The Journal of Adhesion, 20: 2, 117 — 127
To link to this Article: DOI: 10.1080/00218468608074942
URL: http://dx.doi.org/10.1080/00218468608074942

J. Adhesion, 1986, Vol. 20, pp. 117–127
0021-8464/86/2002-0117 $18.50/0

Printed in the United Kingdom

Nickel Activated Phosphating of Cold-Rolled Steel

H. W. K. ONG, L. M. GAN and T. L. TAN

Chemistry Department, National University of Singapore, Republic of Singapore

(Received January 3, 1986; in final form February 4, 1986)

Phosphating of cold-rolled steel was investigated. A dense, uniform and fine-grained zinc phosphate crystalline layer was observed after nickel activation. These crystalline layers were shown to have improved strength, durability and corrosion resistance. The mechanism of the growth of the zinc phosphate layer is discussed.

KEY WORDS Cold-rolled steel; corrosion resistance; durability; mechanism of nickel activation; nickel-activated phosphating; phosphate nucleation.

INTRODUCTION

The corrosion protection by zinc phosphate coating on steel surface depends essentially on the nature of its phosphate crystallites, its texture and adhesion strength. The phosphate coating deposition involves a crystallization process[1–4] at active nucleation sites[5] found on the steel surface. This protective layer should consist of many crystallite growths uniformly distributed over the steel surface and densely packed in order to enhance the resistance of the steel to corrosion.

The phosphate nucleation and its subsequent growth are greatly influenced by the physical consistency of the steel surface.[6–8] Surface treatment of cold rolled steel prior to phosphating has an appreciable influence on the rate of the phosphate crystal growth[9–10] and its structure. The number of active sites present within the surface heterogeneity is decisive in controlling the nucleation process.

Pretreatment of steel surface involving a complex titanium solution or oxalic acid has been reported[11] to favour the formation of a dense and fine-grained phosphate deposition. This is attributed to the adsorption of very small atomic titanium particles on the steel surface. The adsorption of titantium particles increases the active sites giving a denser nucleation and hence the growth of a finer-grain phosphate crystal layer.

The chemical activation mechanism for phosphating is not yet well understood. This paper discusses the phosphating on cold rolled steel surface activated by a nickel solution. The growth, structure and strength of the phosphate crystal obtained from such an activated system will be examined together with its corrosion resistance.

EXPERIMENTAL

Cold rolled steel panel phosphating

A number of zinc phosphate solutions including different nickel compounds were first formulated for evaluation in terms of the formation of a uniform, fine-grained and densely packed coating. Two types, system A and system B, were finally chosen for the study of the effect of a nickel activator on the phosphate nucleation and growth. System A consisted of a solution of 22.5 g ZnO, 20 g $NaNO_3$, 50 ml H_3PO_4, and 50 ml distilled water, while system B contained 2.5 g $Ni(NO_3)_2 \cdot 6H_2O$ in addition to solution A.

Panels of cold rolled steel (CRS) 101.60 × 25.40 × 0.63 mm were first degreased and washed in a 5% trisodium phosphate/1% Teepol solution at 80°C. The cleaned panels were then etched in dilute hydrochloric acid (2 M) for 3 minutes, washed with warm distilled water and conditioned in an oven at 90°C for 20 minutes. These etched panels were subsequently phosphated in 3% stock phosphating solution of system A or B at 75°C for varying periods of time. Phosphated CRS panels were rinsed with distilled water followed by a 10 seconds immersion in a 0.2% chromic acid solution. After a few more rinses with distilled water, the panels were placed in an oven at 90°C for 24 hours before the coating weights were recorded.

Cold rolled steel surface for SEM examination

The surfaces of CRS pieces 3 × 3 mm, mounted on a thermoplastic holder, were polished by fine grade carbide paper and diamond paste to produce a final mirror-finish surface of minimum grinding marks. They were alkaline washed prior to phosphating. In order to remove any loosely adherend particles, the phosphated specimens were subjected to two minutes wash by acetone in an ultrasonic bath. They were immediately stored in a desiccator and were examined under the Joel-35CF electron microscope at 8000 magnification. Surface components of the phosphate layer were also analysed by an Energy Dispersion Spectrometer.

Phosphate strength and corrosion resistance

The shear strength of the phosphate crystal layer was measured by forming a lap joint composite with silicone as reported previously.[9–10] The resulting lap joints with 2.00 × 2.54 cm overlap were cured for 14 days at room temperature and they were pulled apart by a tensile tester (Instron 1026).

A series of panels which had 8 minutes phosphating were exposed to outdoor and laboratory conditions with twice weekly salt spray on them to determine the severity of rust formation.[12] These panels were examined daily and the rust formation was reported using the scale specified in ASTM D1654.

RESULTS

Activated coating characteristics

The rates of nickel activated (system B) and non-activated (system A) phosphating on the dilute hydrochloric acid etched CRS are shown in Figure 1. After about 5 minutes of phosphating, the rate of coating weight per unit time slowed down considerably for both systems. The saturated coating weight for the nickel activated system was about 17 g/m^2 while 11 g/m^2 was obtained for the non-activated solution. When the phosphate coating weight was plotted against the phosphating time in log scale, a pair of two straight lines was observed for both systems as shown in Figure 2. These lines indicate that phosphate deposition proceeded in two

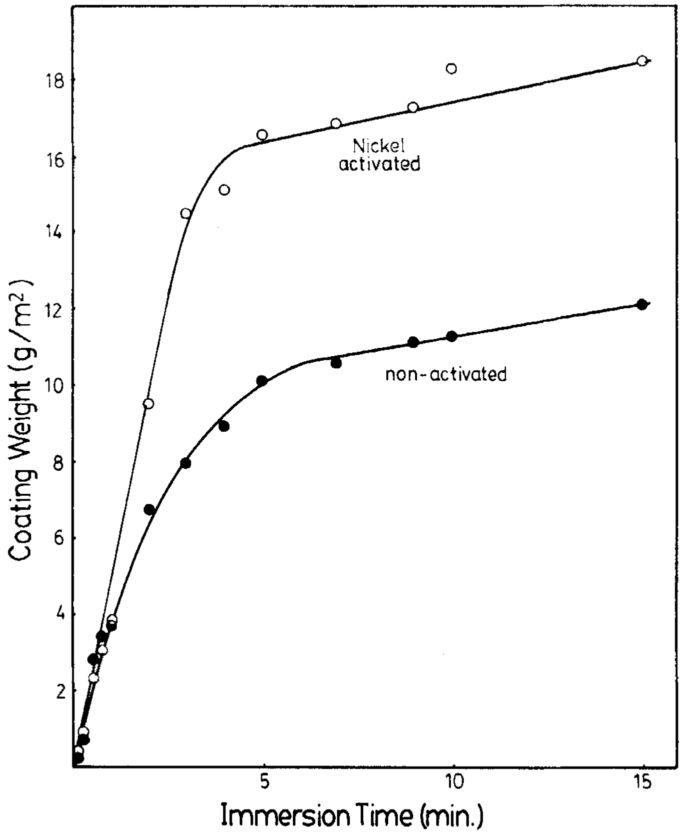

FIGURE 1 Kinetics of phosphating on the CRS surfaces etched with dilute HCl.

stages. The rate of primary phosphate deposition was about the same for both systems, but the secondary phosphate deposition was about twice as fast for the nickel activated system. Nickel activator could have activated more sites on CRS surface for phosphate nucleation in the first-stage growth. With this increased number of phosphate nucleation sites, a faster, uniform and dense growth of second-stage crystals could be expected after prolonged phosphating.

In addition, electron micrographs (Figure 3a and 3b) of the metallurgically polished CRS surfaces reveal the different secondary

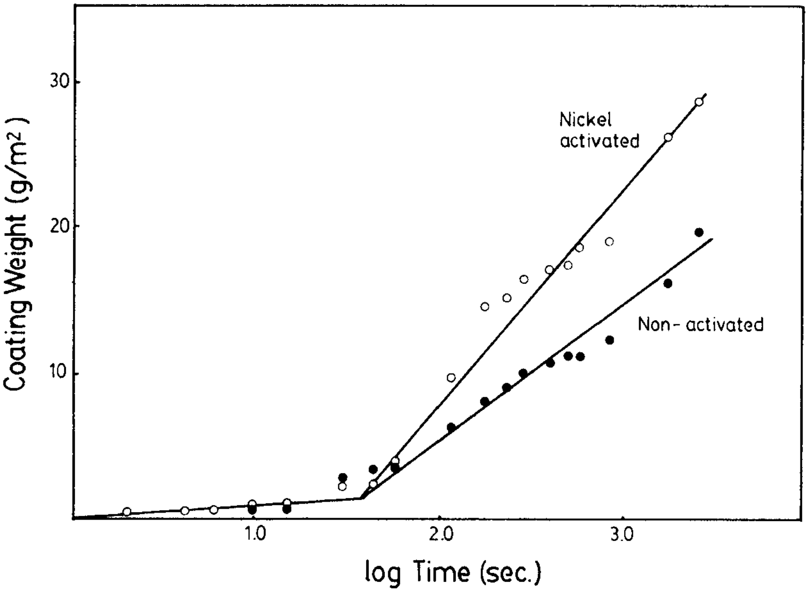

FIGURE 2 Deposition of phosphate on CRS etched with dilute HCl.

platelet structures growing from the primary phosphate crystals after 45 seconds of immersion phosphating. It is also noted that the secondary phosphate deposition of the nickel activated system produced a denser coverage of CRS surface compared with that obtained from the non-activated system.

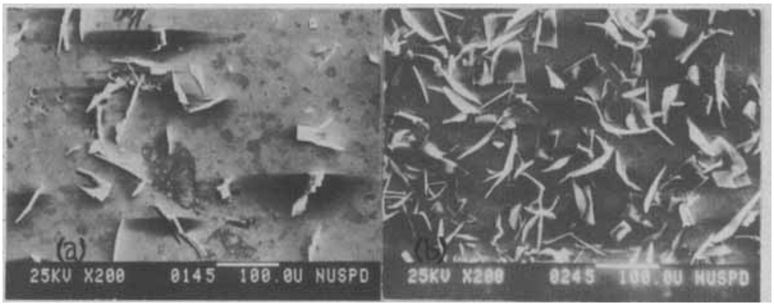

FIGURE 3 (a) A sparsely distributed growth of secondary platelet phosphate crystals after 45 sec of non-activated phosphating. (b) A more dense secondary growth of platelet crystals after 45 sec of nickel-activated phosphating.

TABLE I
Lap shear strength of phosphated CRS-silicone composite

Phosphating time (sec.)	Non-activated system	Nickel activated system
	Mean shear strength (kN/m)	
5	695.2	727.4
15	682.3	817.4
30	704.8	824.0
60	795.0	907.6
180	740.2	749.9
300	711.2	704.8
4800	650.2	643.6

Means of 4 determinations; *C* of *V* ~3%.

The strength of the phosphate crystals deposited on CRS was evaluated from the rupture of the lap joint bonded with silicone sealant. Since a cohesive failure within the phosphate crystal was observed for all phosphated composites, the shear strengths obtained were regarded as the strengths of the phosphate crystals, as shown in Table I.

For short-time phosphating up to 1 minute, the primary first-stage phosphate crystals formed in the nickel activated solution led to a significantly higher strength than those non-activated ones. The maximum shear strength of primary phosphate crystal was about 900 kN/m for the former and 800 kN/m for the latter. No difference in secondary crystal strength was observed for either system when the phosphating period exceeded 3 minutes. The shear strength was measured to be about 750 kN/m for both systems at 3 minutes phosphating. This strength was 50% higher than that obtained previously by using the commercial phosphating solutions.

Electron micrographs of the CRS surfaces etched with dilute hydrochloric acid show that after 3 min of phosphating, the activated system produced a uniform and densely packed phosphate crystal layer (Figure 4a). Upon prolonged phosphating to 15 min, a mixed structure was observed comprising secondary platelets and dendritic crystals (Figure 4b).

This mixed structure of phosphate deposited on CRS surface was found to improve corrosion resistance. Table II shows the exposure

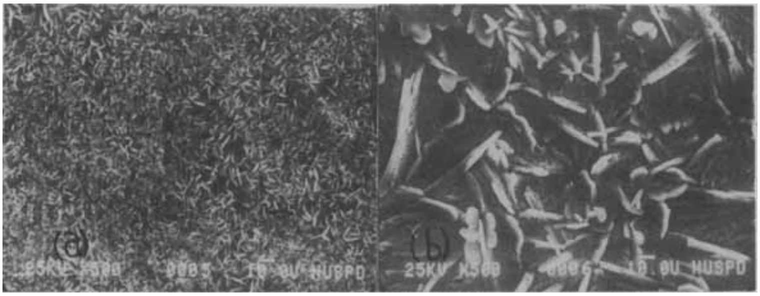

FIGURE 4 (a) A uniform, densely packed growth of fine-grained secondary crystals after 3 min of nickel-activated phosphating of CRS etched with dilute HCl. (b) A mixed secondary growth of platelet and dendritic crystals after 15 min of nickel-activated phosphating of CRS etched with dilute HCl.

performance against rust formation for the activated and non-activated phosphating systems. It is clearly shown that nickel activated phosphating system provides better corrosion resistance.

Mechanism of nickel activation

The scanning electron micrographs of the polished CRS after being phosphated in the nickel activated and non-activated solutions are presented in Figure 5. Figure 5a reveals the unphosphated CRS surface with abrasive marks. Upon immersion in the non-activated phosphating solution for 30 seconds, nucleation/growth of primary phosphate crystals can be observed from Figure 5b to be sparse and

TABLE II
Comparison of rust formation

Phosphating for 8 min.	Exposed condition	Length of exposure (days) 1	2[a]	3	4	5[a]	6	7
		ASTM D1654 Scale						
Non-	Indoor	10	10	8	6	3	1	1
activated	Outdooor	10	9	7	4	3	0	0
Nickel	Indoor	10	10	10	8	6	6	4
activated	Outdoor	10	10	9	7	5	3	3

[a] Salt-spray (5% sodium chloride solution).

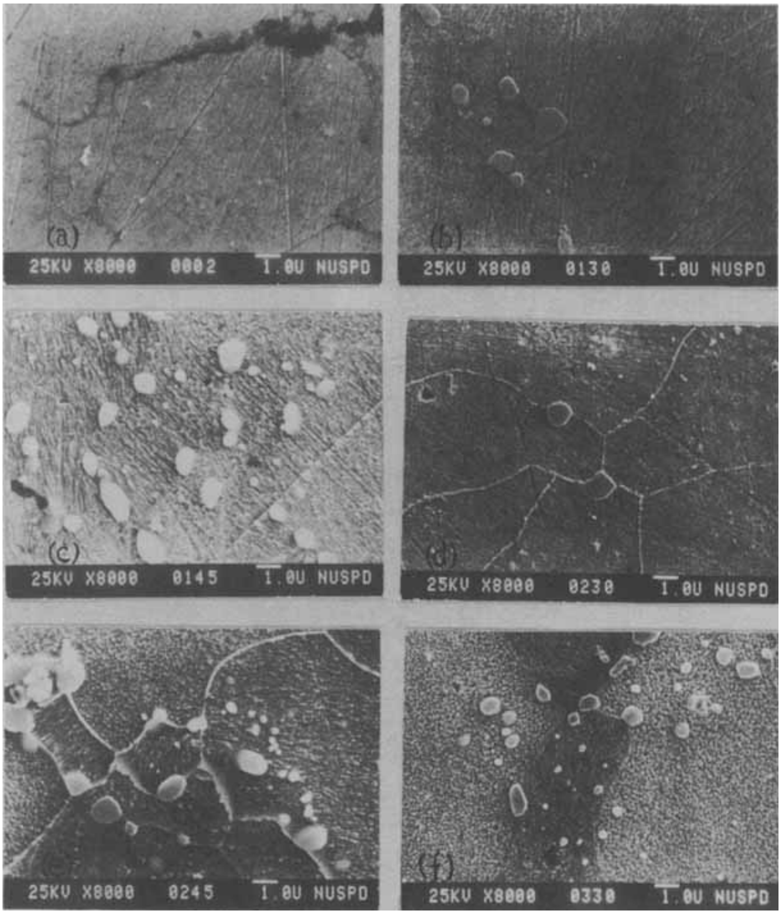

FIGURE 5 Scanning electronmicrographs of phosphated CRS. (a) Polished CRS before phosphating and showing marks of abrasive. (b) Nucleation of primary phosphate crystals on polished (but not etched) CRS by non-activated solution after 30 sec. (c) Growth of phosphate crystals from (b) after 45 sec. (d) Nucleation of phosphate crystals along grain boundaries by nickel-activated solution after 30 sec. (e) As (d) but after 45 sec showing growth of wall-like structure along the grain boundaries. (f) The formation of uniform and densely packed phosphate layer on CRS etched with HCl in non-activated solution after 30 sec.

randomly distributed. After 45 seconds of non-activated phosphating, there was an enhanced primary growth but the distribution remained sparse with the abrasive marks still visible as shown in Figure 5c. With nickel activated phosphating, there was a clearly defined and denser primary growth along the grain boundaries after 30 seconds (Figure 5d). At 45 seconds of immersion (Figure 5e), the grain boundary growths became wall-like structures dispersed with some droplet-like growths.

For phosphating on an HCl-etched CRS surface by the non-activated solution, a uniform and densely packed layer of phosphate crystals was observed as in Figure 5f. It differed from the wall-like structure along the grain boundaries (Fig. 5e) obtained by phosphating the polished CRS surface in the nickel activated solution. The exposure of the grain boundaries by acid etching would have produced the similar wall-like structure if the presence of nickel activator simply provided more active sites for phosphating. However, this wall-like structure phenomenon was not observed with the acid etched surface for non-activated phosphating. This indicates that nickel activator plays an important role in affecting the structure of phosphate growth besides creating more active sites for phosphating.

The uncoated CRS surface was analysed by X-ray Dispersion Spectrometry and found to consist of 4.69% Cu, 0.46% Mn, 0.32% Cr and 92.62% Fe. These elements together with carbon were randomly distributed over the CRS surface. All the phosphated panels showed generally higher iron counts than the unphosphated panels. This could be due to the initial iron dissolved from the CRS surface being trapped in the deposited phosphate layers. Besides the obvious influence of surface cleanliness and the topography effects upon phosphate deposition, the presence of even a thin layer of carbon deposits is believed to prevent the formation of a phosphate layer making it susceptible to corrosion. The reason for this is that incomplete coverage of surface caused by the existence of carbon can act as reactive sites for initiation of the oxidation and reduction reactions. It is difficult to eliminate the existence of surface carbon deposits but in our examination of cold rolled steel surfaces, these surface carbon deposits were found to be randomly distributed and not confined to specific areas.

DISCUSSION

A growth mechanism for the nickel activated phosphating is proposed as shown schematically in Figure 6. It is envisaged that the nickel activator increased the number of active phosphating sites on CRS, especially along the grain boundaries. The subsequent nucleation/growth of primary phosphate at the grain boundaries leading to the formation of the wall-like structures was therefore very rapid. The wall-like structures continued to grow into the

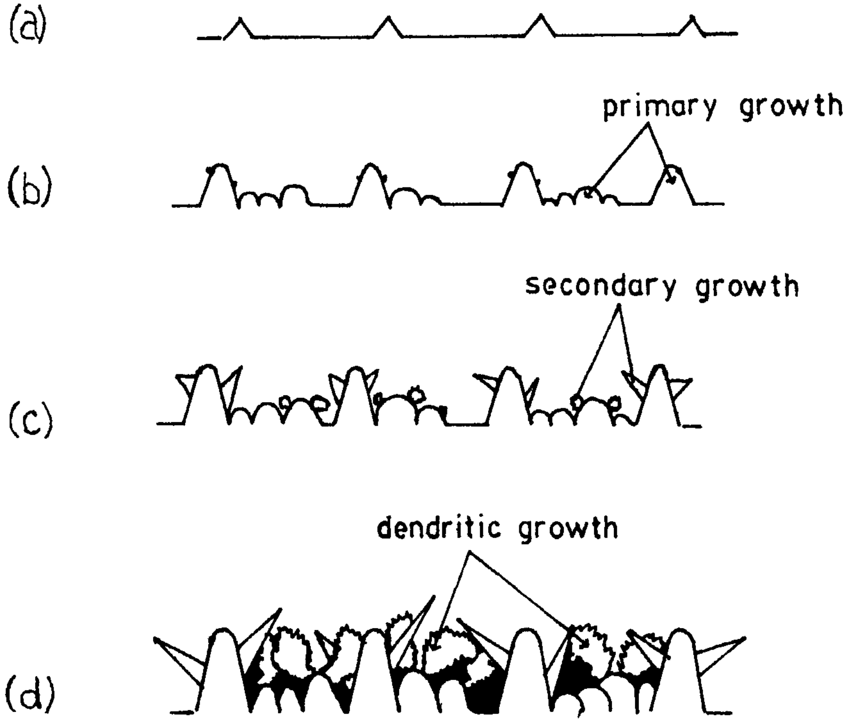

FIGURE 6 Schematic diagram for nickel-activated phosphate crystal growth on cold-rolled steel surfaces. (a) Active sites along the crain boundaries of CRS. (b) Nucleation and growth of primary zinc phosphate crystals along the grain boundaries is greater than that within boundaries. (c) Appearance of secondary phosphate platelet crystals along the grain boundaries. (d) Secondary dendritic growth of phosphate crystals on the primary phosphate layer resulting in the mixed phosphate structures on the CRS surface.

secondary platelet structures. On the other hand, nucleation/growth within the grain boundaries was in the form of spots of 0.1–0.5 micron in diameter after 45 seconds phosphating (Figure 5e). These grew to about 1–2 microns effectively covering the CRS surface with a dense and uniform layer before secondary dendritic phosphate growth emerged.

The proposed mechanism would account for the mixed phosphate crystal structures observed in Figure 4b and the increased strength of phosphate crystal obtained. Nucleation/growth of the phosphate crystals at grain boundaries and within the grains would proceed at varying rates and this would give rise to an honeycombed surface structure for the short-period phosphating. The complexity of this activated growth structure would contribute to an increase in shear strength of the lap joint composite.

In conclusion, by employing nickel activator in the phosphating process, it is possible to increase the rate of phosphate deposition, its strength and its corrosion resistance. In turn, uniform and stronger phosphate layer on cold rolled steel surface would improve corrosion resistance when a supplementary organic finish is applied.

Acknowledgement

The authors wish to thank Mrs Phua of the Physics Department for her assistance in preparing the scanning electron micrographs.

References

1. J. V. Laukonis, *Interface Conversion for Polymer Coating,* P. Weiss and G. D. Cheever, Eds. (Elsevier, New York 1968), pp. 182–199.
2. G. D. Cheever, *J. Paint. Technol.* **39,** 504 (1967).
3. J. Bogi and R. Macmillan, *J. Mater. Sci.* **12,** 2235 (1977).
4. L. O. Gilbert, *Tech. Proc. Am. Electroplaters Soc.* **43,** 195 (1956).
5. W. Manchu, *Werstoffe Korrosion* **14**(7), 566 (1963).
6. G. M. Zhang and S. G. Kapor, *Corrosion Sci.* **24,** 977 (1984).
7. E. L. Ghall and R. J. A. Potvin, *Corrosion Sci.* **12,** 583 (1972).
8. R. A. Iezzi and B. Leidheiser, *Corrosion* **37,** (1981).
9. L. M. Gan, H. W. K. Ong and T. L. Tan, *J. Adhesion* **16**(3), 233 (1984).
10. H. W. K. Ong, L. M. Gan and T. L. Tan, *J. Adhesion* **18**(3), 227 (1985).
11. G. Jernstedt, *Trans. Electrochem. Soc.* **83,** 361 (1943).
12. M. J. Crewdson and S. G. Lane, *Met. Finish.* **63,** (Oct.) (1984).